CrossMark

# The influence of surface type on the absorbed radiation by a human under hot, dry conditions

A. W. Hardin[1] · J. K. Vanos[1,2]

**Abstract** Given the predominant use of heat-retaining materials in urban areas, numerous studies have addressed the urban heat island mitigation potential of various "cool" options, such as vegetation and high-albedo surfaces. The influence of altered radiational properties of such surfaces affects not only the air temperature within a microclimate, but more importantly the interactions of long- and short-wave radiation fluxes with the human body. Minimal studies have assessed how cool surfaces affect thermal comfort via changes in absorbed radiation by a human ($R_{abs}$) using real-world, rather than modeled, urban field data. The purpose of the current study is to assess the changes in the absorbed radiation by a human—a critical component of human energy budget models—based on surface type on hot summer days (air temperatures >38.5 °C). Field tests were conducted using a high-end microclimate station under predominantly clear sky conditions over ten surfaces with higher sky view factors in Lubbock, Texas. Three methods were used to measure and estimate $R_{abs}$: a cylindrical radiation thermometer (CRT), a net radiometer, and a theoretical estimation model. Results over dry surfaces suggest that the use of high-albedo surfaces to reduce overall urban heat gain may not improve acute human thermal comfort in clear conditions due to increased reflected radiation.

Further, the use of low-cost instrumentation, such as the CRT, shows potential in quantifying radiative heat loads within urban areas at temporal scales of 5–10 min or greater, yet further research is needed. Fine-scale radiative information in urban areas can aid in the decision-making process for urban heat mitigation using non-vegetated urban surfaces, with surface type choice is dependent on the need for short-term thermal comfort, or reducing cumulative heat gain to the urban fabric.

**Keywords** Absorbed radiation · Urban climate · Thermal comfort · Albedo · Extreme heat · Urban heat island

## Introduction

The expansion and growth of cities in conjunction with projected climate change have the potential to exacerbate urban high-temperature extremes and their associated human health risks. Challenges that cities are confronted with regarding the urban heat island (UHI) intensity—such as energy demands and heat stress vulnerabilities—are dependent on how cities expand and develop (Steeneveld et al. 2011). These challenges underline the need to understand the influence of the built environment on heat exposure at finer scales, which affects human health, well-being, and productivity in cities through thermal comfort (Theeuwes et al. 2015). The cascading effects of urbanization and adaptive demands manifest at various scales in the natural and built environment (Grimm et al. 2008), where improved observations at fine spatial and temporal scales can have valuable information for understanding these effects.

The UHI is a well-known mesoscale phenomenon caused by numerous factors related to land cover, energy use, anthropogenic heat, and the configuration and expanse

✉ J. K. Vanos
jkvanos@ucsd.edu

A. W. Hardin
Aaron.Hardin@ttu.edu

[1] Texas Tech University, Lubbock, TX 79409, USA

[2] Present address: University of California, San Diego, La Jolla, CA 92093, USA

of buildings, with high-heat-retaining materials collecting daytime heat and releasing it overnight (Grimmond et al. 2010; Oke 1987). While it is important to understand the meteorological differences of the ambient environment above impervious and natural surfaces, surface characteristics of radiant temperature and albedo play an important role in the absorbed radiation by a human ($R_{abs}$) and the total thermal stress on a person (Snir et al. 2016). For example, an asphalt versus concrete surface will result in differing total available energy, sensible heat and latent heat fluxes, and thus air temperatures, all of which influence thermal, radiant, and moisture properties of microclimates within a city (Oke et al. 1992). These microclimate variations can significantly affect the thermal comfort of humans through changes in convective and evaporative heat fluxes, and the amount of radiation absorbed by a human (Brown and Gillespie 1986; Krüger et al. 2013; Vanos et al. 2012). An understanding of these properties at a fine scale within complex urban areas is critical information to implement spatially congruent urban adaptation measures to direct UHI mitigation actions (Solís et al. 2016).

Urban dwellers are more prone to suffering from heat-related illnesses or death than those living in rural areas (Tan et al. 2010). According to the most recent National Health Statistics Report, heat-related deaths were the second leading cause of weather-related deaths between 2006 and 2010 in the USA (Berko et al. 2014). Large variations in heat vulnerability affect how humans respond and adapt to heat, due in large part to variable design, as well as socioeconomic factors such as education, poverty rates, and access to air conditioning (Harlan et al. 2006). Recent research has identified that within neighborhoods and microclimates, differences in surface temperatures and ambient characteristics can vary significantly, particularly on the warmest days (Chow et al. 2012; Vanos et al. 2016; Jenerette et al. 2015). These differences are primarily attributable to non-uniform gains in solar radiation, and have implication for human thermal comfort.

The combination of all short- and long-wave radiant fluxes in a given point location results in a mean radiant temperature ($T_{mrt}$) (Thorsson et al. 2007; Kenny et al. 2008), which is the most significant heat gain to urban surfaces and human heat load on warm-hot days. Therefore, accurate radiation monitoring or modeling is required for assessing the thermal environment's influence on human heat stress. Numerous models exist to estimate the energy budget of a human in a given environment (see Vanos et al. 2010; Chen et al. 2012). These models generally assess a combination of vapor pressure, air temperature, mean radiation load, and wind speed to model the energy streams of convection, evaporation, radiation, and metabolism towards and away from a human.

In situ observation to understand thermal comfort is a common area of research within Europe (e.g., Ketterer and Matzarakis 2014; Matzarakis et al. 2011; Thorsson et al. 2007) and select North American cities (e.g., Middel et al. 2014), yet such information is comparatively limited in North America. Moreover, the majority of research examining urban heat-health risks in the USA is often based on sparse standardized meteorological observations characterizing the mesoscale variation in urban climate (Kuras et al. 2015; Kuras et al. 2017), which gives little evidence of the linkages between urban form, temperature, and human health (Theeuwes et al. 2015). Probable reasons for the lack of urban microclimate evidence is due to the expensive nature of high-end meteorological stations with net radiometers, the difficulty in safely setting up stations in areas where humans prevail, and the complexity in processing the data. The current study attempts to overcome these limitations by comparing three methods of radiation prediction/measurement to test lower-cost methods over various urban surfaces during days of extreme heat. Just as these surfaces will have their own unique energy budget, the humans that stand on these surfaces will also have their own energy budget, where the major energy streams affecting a human budget (Brown and Gillespie 1986; Fanger 1970) can be quantified. Understanding the various flux components to and from a human body, specifically the influence of radiation on the human energy budget, can provide directed strategies for reducing localized heating and thus heat stress.

The current study examines radiation balances over various urban surfaces in order to estimate $R_{abs}$. The goal is to examine the radiational environments experienced by a human over ten common urban surfaces during high temperatures (air temperature ($T_a$) >38 °C) and high sky view factors (SVFs) in the semi-arid climate zone of Lubbock, Texas. We first calculate and statistically compare three methods to estimate the $R_{abs}$ by a human in each microclimate, and second, determine the variations in radiation balances and $R_{abs}$ over the various surfaces and how the balances (e.g., long-wave versus short-wave incoming and outgoing) affect the $R_{abs}$. This analysis provides quantitative information pertaining to urban heating due to radiation absorption and the subsequent impacts on the human energy budget (and thus thermal comfort) that can lead to heat stress.

## Data and methods

### Field tests

Microclimate data were collected using a portable weather station situated over ten surfaces on 13 days (Table 1)

**Table 1** Date, surface, weather type (dry tropical - DT; moist tropical, MT), and description of each portable weather station deployment

| Surface | Date | SSC | Description |
| --- | --- | --- | --- |
| Dry grass | 6/29/14 | DT | Open yard with short Bermuda grass. |
| Sand | 6/30/14 | DT | White sand volleyball court. |
| Wet grass | 7/14/14 | MT | Urban park in residential neighborhood with short Bermuda grass. |
| Asphalt | 8/06/14 | DT | Asphalt parking lot with no cars. |
| School blacktop | 8/07/14 | DT | Asphalt surface at elementary school. |
| Tennis court | 8/08/14 | DT | Green painted tennis court (asphalt). |
| Concrete | 8/24/14 | DT | Tan concrete roof of 4-story parking garage with no cars. |
| Gray roof 1 | 8/26/14 | MT | Gray roof of 12-story building. |
| Gray roof 2 | 8/31/14 | DT | Gray roof of 12-story building. |
| Artificial turf | 9/01/14 | DT | Green artificial turf with small black rubber pellets. |
| Green roof 1 | 9/02/14 | DT | Tall brown switchgrass with some visible soil. |
| Green roof 2 | 9/03/14 | MT | Tall brown switchgrass with some visible soil. |
| Green roof 3 | 9/04/14 | MT | Short green grass with some visible dark soil. |

throughout the summer months of 2014 in Lubbock, Texas (33.57° N, 101.88° W). Lubbock is situated in a semi-arid climate with mean daily maximum summer temperatures of 33.3 °C (92 °F) and predominantly clear skies. Data were generally collected from midday to the late afternoon, and thus, we performed analyses on data collected between 1300 and 1800 h local standard time to maintain consistency between days. The portable weather station (Fig. 1) consisted of an R.M. Young Model 05305 anemometer with propeller for wind speed and direction, a Campbell Scientific CNR4 net radiometer measuring incoming and outgoing long-wave and short-wave radiation, a Campbell Scientific HMP45C air temperature ($T_a$) and relative humidity (RH) probe, and a cylindrical radiation thermometer (CRT) measuring the radiant temperature. Data were recorded using a Campbell Scientific CR3000 micrologger at 30-s intervals.

The station was deployed when an oppressive weather type (dry tropical (DT) or moist tropical (MT); Sheridan (2002)) was forecasted to arrive, or the maximum $T_a$ was forecasted to be at or above 100 ° F. A DT weather type was present on nine of the 13 study days, with an MT weather type present on the remaining four (see Table 1). The spatial synoptic classification (SSC) provides a way to monitor commonality in weather conditions between the deployments, allowing for improved comparisons of the data given low variability in the air temperatures.

The CRT (small tan cylinder displayed in Fig. 1) is a copper cylinder (10-cm height and 1.0-cm diameter) filled with conductive epoxy with a copper-constantan thermocouple inserted in the middle. It is designed to have the representative geometry (cylinder) and radiational properties of an average clothed human (albedo of 0.39 and emissivity of 0.95) (Brown and Gillespie 1986; Kenny et al. 2008;

**Fig. 1** Portable weather station over artificial turf and a green roof in Lubbock, TX

Monteith 1973). The CRT measures a value of radiant temperature that is then used to provide a value of $R_{abs}$ (Wm$^{-2}$), which is an integration of the total solar and terrestrial radiation fluxes that are absorbed by a cylindrical body (Kenny et al. 2008). The CRT was designed by Brown and Gillespie (1986) and was further updated by Krys and Brown (1990) and Kenny et al. (2008), with outdoor applications by Kenny et al. (2009a) and Vanos et al. (2012a).

Due to a HMP45C sensor malfunction, $T_a$ and RH data from the portable station are unavailable from 8/24/14 onwards. For the dates of 8/26/14 and 8/31/14 (gray roof), the $T_a$ and RH data were obtained from a long-term weather station (Davis Vantage Pro 2) on the same rooftop, approximately 10 m from the portable station. For the dates of 09/01/14 (artificial turf) and 09/02/14–09/04/14 (green roof), $T_a$ and RH data were obtained from the Lubbock Weather Forecast Office (WFO) meteorological station, located approximately 2.5 km from each location. As air temperature variations across the city (16 km) were 0.5–2.0 °C based on observations at intraurban weather stations and the airport, the difference in the $T_a$ and RH observations from the WFO to the given surface is expected to be small. Additionally, $T_a$ and RH vary minimally across a large area and are difficult to modify with urban design due to the efficiency of wind at mixing heat and moisture, whereas the wind speed and radiation are easily modified and thus have a great impact at the microscale (Brown and Gillespie 1995).

## Calculation of radiation absorbed by a human

The total radiation absorbed by a human depends on incoming short-wave radiation ($K_{in}$), reflected short-wave radiation ($K_{up}$), incoming long-wave radiation ($L_{in}$), and emitted long-wave radiation from the ground ($L_{up}$). Here, we use three different methods to calculate the $R_{abs}$ by a human based on ambient conditions over various but common urban surfaces: (1) a theoretical estimation model ($R_{est}$) based on the basic principles of atmospheric radiation requiring no direct measurements, (2) horizontal short- and long-wave radiation measurements provided by the CNR4 net radiometer ($R_{cnr}$), and (3) a simple cylindrical radiation thermometer ($R_{crt}$) as in Kenny et al. (2008). The simultaneous deployment of a CNR4 and CRT offers a unique opportunity to compare methods of calculating $R_{abs}$ in hot conditions. For each method, we model a human after a cylinder for proper geometric representation, and hence, a more accurate estimate of the absorption of short- and long-wave radiation (Brown and Gillespie 1986; Krys and Brown 1990; Kántor and Unger 2011; Holmer et al. 2015).

This subsection is presented as follows: we first present the theoretical equations used to estimate incoming and outgoing radiation fluxes; second, we determine components of direct beam and diffuse short-wave radiation using the

CNR; third, we present the equations used to determine $R_{abs}$ by a cylinder based on inputs from either theoretical estimations or values from CNR measurements (Eqs. 9–14); finally, we provide the calculation of $R_{abs}$ using the CRT.

The theoretical estimation of absorbed radiation, $R_{est}$, first models the radiation received on a horizontal surface (Eqs. 1–8). The beam component of the solar radiation ($K_b$) incident on a horizontal surface is estimated as follows:

$$K_b = K_p \cos(\psi), \tag{1}$$

where $K_p$ is the incoming direct radiation received perpendicular to the beam (Campbell and Norman 1998) and $\psi$ is the zenith angle (°), calculated every minute.

The incoming direct irradiance received on a surface perpendicular to the beam is as follows (Campbell and Norman 1998):

$$K_p = K_o \tau^m, \tag{2}$$

where $K_o$ is the solar constant defined as the amount of radiation hitting the top of Earth's atmosphere on a plane surface normal to the solar beam (1367 Wm$^{-2}$) (Oke 1987), $\tau$ is the atmospheric transmittance, and $m$ is the optical air mass number. For zenith angles less than 80°, $m$ can be estimated as Campbell and Norman (1998):

$$m = \frac{P_a}{101.3 \cos(\psi)}, \tag{3}$$

where $P_a$ is atmospheric pressure (kPa). Because pressure was not directly measured, the $P_a$ was calculated using the following equation (Campbell 1977):

$$P_a = P_o e^{\frac{-A}{8200.0}}, \tag{4}$$

where $P_o$ is sea level pressure (101.3 kPa) and $A$ is altitude in meters.

Transmissivity was calculated by determining the root mean square error (RMSE) (Eq. 20) between estimated $K_{in}$ and $K_{up}$ from the CNR4 with different ranges of $\tau$, as in Kenny et al. (2008). The $\tau$ value with the smallest error was then chosen as the value for a given day, and hence, we have a single $\tau$ for each deployment. Values are listed in Table 2.

To estimate the incoming diffuse radiation ($K_d$) in the theoretical estimation model, we calculate $K_d$ as follows (Campbell and Norman 1998; van den Brink et al. 2016):

$$K_d = 0.3(1 - \tau^m)K_o \cos(\psi). \tag{5}$$

For clear days, we also assume that $K_{in} = K_b + K_d$, and on full overcast days (June 29, 2014 in the current study), we assume $K_{in} = K_d$.

For the estimation model of absorbed radiation (i.e., $R_{est}$), incoming and outgoing long-wave radiation ($L_{in}$ and $L_{up}$) were estimated based on a linear approximation of the dependence of full radiation on temperatures above 283 K developed by Monteith and Unsworth (1990). The equations

**Table 2** Average values of $T_a$ (°C), $T_{crt}$ (°C), $\Delta T_{c-a}$ (°C), $\tau$ (%), wind speed $V$ (ms$^{-1}$), $R_{cnr}$ (Wm$^{-2}$), $R_{crt}$ (Wm$^{-2}$), $R_{est}$ (Wm$^{-2}$), and energy budget (B) (Wm$^{-2}$) for each surface. The energy budget values in parentheses signify the modeling of the given physical activity listed in the methods section 'Energy budget analysis'

| Surface | $T_a$ | $T_{crt}$ | $\Delta T_{c-a}$ | $\tau$ | $V$ | $R_{cnr}$ | $R_{crt}$ | $R_{est}$ | B |
|---|---|---|---|---|---|---|---|---|---|
| Dry grass | 38.8 | 40.6 | 1.8 | 66 | 1.04 | 547.9 | 455.2 | 486.6 | 226.1 (398.2) |
| Sand | 36.6 | 41.8 | 5.2 | 68 | 3.02 | 557.2 | 647.5 | 496.3 | 242.3 (440.9) |
| Park—moist grass | 32.6 | 34.0 | 1.4 | 38 | 0.83 | 446.2 | 405.3 | 395.1 | 113.6 (152.3) |
| Asphalt | 35.2 | 36.7 | 1.5 | 70 | 3.57 | 540.6 | 454.9 | 481.3 | 206.5 |
| School blacktop | 37.3 | 39.3 | 2.0 | 66 | 1.90 | 558.6 | 470.5 | 492.8 | 234.0 (428.3) |
| Tennis court | 35.4 | 38.7 | 3.3 | 60 | 1.52 | 533.9 | 500.4 | 461.9 | 208.6 (315.3) |
| Concrete | 34.7 | 36.6 | 1.9 | 64 | 2.00 | 549.8 | 457.5 | 504.0 | 220.0 |
| Gray roof 1 | 33.4 | 35.1 | 1.8 | 56 | 1.15 | 525.9 | 423.6 | 476.1 | 195.1 |
| Gray roof 2 | 36.2 | 36.8 | 0.6 | 66 | 1.67 | 558.9 | 405.8 | 492.8 | 230.6 |
| Artificial turf | 37.0 | 38.7 | 1.7 | 69 | 3.25 | 535.3 | 480.1 | 473.3 | 225.7 (416.7) |
| Green roof 1 | 34.4 | 36.5 | 2.1 | 60 | 1.78 | 503.9 | 456.1 | 474.0 | 175.5 |
| Green roof 2 | 32.3 | 34.2 | 1.9 | 68 | 2.88 | 523.6 | 460.3 | 470.9 | 190.1 |
| Green roof 3 | 30.3 | 31.8 | 1.5 | 65 | 4.25 | 535.3 | 439.4 | 458.8 | 194.2 |

for estimating incoming long-wave radiation ($L_{in}$) and outgoing long-wave radiation ($L_{up}$) (Wm$^{-2}$) are as follows:

$$L_{in} = 213 + 5.5 T_a \tag{6}$$

$$L_{up} = 320 + 5.2 T_a. \tag{7}$$

These equations are commonly employed when only the $T_a$ is known, and hence, they are merely used in the current analysis for the $R_{est}$ model.

The net radiometer is considered the most reliable means of collecting radiation data because it measures both direct solar (combined beam and diffuse) sky and ground radiation (pyranometer), as well as sky and terrestrial radiation (pyrgeometers) (Brock and Richardson 2001). For the values measured by the CNR, we break up the incoming beam (direct) and diffuse (isotropic) components of the $K_{in}$ recorded by the CNR (Monteith and Unsworth 1990). This is accomplished using the ratio of $K_d/K_b$ and $K_d = K_{in} - K_b$ in combination with Eqs. 1, 2, and 5, giving us the following ratio (Kenny et al. 2008):

$$K_b = \frac{K_{in}}{1 + \frac{0.3(1-\tau^m)}{\tau^m}}. \tag{8}$$

For the overcast day in the CNR model, we again assume $K_{in} = K_d$.

With the four components of radiation (i.e., $K_{in}$, $K_{up}$, $L_{in}$, and $L_{up}$) estimated theoretically as provided by the above equations, or measured by the CNR, we can now make use of a mathematical interpretation to represent the amount of radiation absorbed by a human.

A vertical cylinder is typically used to model a human in a standing position (Brown and Gillespie 1986; Krys and Brown 1990), where the view factor of the cylinder is 0.5

since any point on the cylinder can only "see" half of the sky and half of the ground hemisphere.

Using the cylinder concept, we calculate the absorbed $K_b$ and $K_d$ (W) as follows (Kenny et al. 2008):

$$K_{b(abs)} = (1 - \alpha_h) K_p \sin(\psi) A_{cs} \tag{9}$$

$$K_{d(abs)} = 0.5(1 - \alpha_h) K_d A_{cyl}. \tag{10}$$

where $A_{cs}$ is the vertical cross-sectional area of the cylinder (m$^2$) and $\alpha_h$ is average skin and clothing albedo (0.39). Equations 9 and 10 are summed to give $K_{in(abs)}$. Absorbed reflected radiation is calculated as follows:

$$K_{up(abs)} = 0.5(1 - \alpha_h) K_{up} A_{cyl} \tag{11}$$

$$L_{in(abs)} = 0.5 \epsilon_h K_{in} A_{cyl} \tag{12}$$

$$L_{up(abs)} = 0.5 \epsilon_h K_{up} A_{cyl}, \tag{13}$$

where $A_{cyl}$ is the surface area of the cylinder and $\epsilon_h$ is the emissivity of a human (0.95). From the above, the total radiation absorbed by a human ($R_{abs}$), in Wm$^{-2}$, is calculated as follows (Vanos et al. 2012):

$$R_{abs} = A_{eff} \frac{K_{in(abs)} + K_{up(abs)} + L_{in(abs)} + L_{up(abs)}}{A_{cyl}}, \tag{14}$$

where $A_{eff}$ is the effective area factor, which is 0.78 for a standing human, accounting for irregularities in the human body (Campbell and Norman 1998).

Finally, we calculate $R_{abs}$ through the use of the CRT ($R_{crt}$). The $R_{crt}$ is modeled based on the assumption that the radiation absorbed by the cylinder equals the radiation emitted by the cylinder.

The radiation absorbed by the cylinder ($Wm^{-2}$) is calculated as follows (Brown and Gillespie 1986):

$$R_{crt} = \epsilon\sigma(T_{crt} + 273.15)^4 + \rho C_p \frac{(T_{crt} - T_a)}{r_m}, \qquad (15)$$

where $\epsilon$ is the emissivity of the cylinder (0.95), $\sigma$ is the Stefan-Boltzman constant ($5.67 \times 10^{-8}$ $Wm^{-2}$ $K^{-4}$), $\rho C_p$ is the volumetric heat capacity of air (1212 $Jm^{-3}$ $K^{-4}$), and $T_{crt}$ is the temperature of the CRT (°C). The resistance of the cylinder to sensible heat transfer, $r_m$ ($sm^{-1}$), is determined by Kenny et al. (2008):

$$r_m = \frac{D}{A Re^n Pr^{0.33} k}, \qquad (16)$$

where $Re$ is the Reynolds number ($VD\nu^{-1}$), $Pr$ is the Prandtl number (0.71), $D$ is the diameter of the cylinder (0.01 m), $V$ is the wind speed ($ms^{-1}$), $\nu$ is kinematic viscosity of air ($1.5 \times 10^{-5}$ $m^2$ $s^{-1}$), $k$ is thermal diffusivity of air ($22 \times 10^{-6}$ $m^2$ $s^{-1}$), and $A$ and $n$ are empirical constants derived from experiments on heat flow from cylinders: if $Re < 4000$, $A = 0.683$, and $n = 0.466$; if $Re > 4000 < 40{,}000$, $A = 0.193$ and $n = 0.618$; and if $Re > 40{,}000$, $A = 0.0266$, and $n = 0.805$ (Kreith and Black 1980). The Prandtl number is considered constant because it is independent of temperature and only heat transfer through air, not any other gas (Monteith and Unsworth 2008).

These methods have only been tested over grass in fair-weather conditions in the temperate city of Guelph, ON Canada (24.0 °C) by Kenny et al. (2008), and hence, the current study provides information on the validity of the methods during extreme heat ($T_a > 100$ °F). We further compare the three methods using $R_{abs}$ values for input into a human energy budget equation (i.e., we multiply by the $A_{eff}$), and hence, results are not directly comparable to that of Kenny et al. (2008).

### Energy budget analysis

The human energy budget ($B$) was calculated over each surface using Eq. 17, summing the energy streams towards and away from the body utilizing the COMFA energy budget model (Kenny et al. 2009a; Brown and Gillespie 1986; Vanos et al. 2012a).

$$B = M + R_{abs} - E - C - L_{emit}, \qquad (17)$$

where $E$ and $C$ are evaporative and convective heat losses, respectively, $L_{emit}$ is long-wave emitted by the body, $R_{abs}$ is calculated using the CNR measurements as outlined in "Calculation of radiation absorbed by a human" section, and $M$ is metabolic heat load ($Wm^{-2}$). Equations used to determine each energy flux can be found in Vanos et al. (2012a), Brown and Gillespie (1986), Kenny et al. (2009a) and

Kenny et al. (2009b). We estimate the energy budget of an average human standing with a metabolic activity ($M_{act}$) of 87 $Wm^{-2}$ (1.5 METs), and a clothing insulation of 0.34 clo (T-shirt, light athletic shorts, socks, shoes) (ISO9920 2007). For surfaces on which physical activity often occurs, we also estimate the $B$ for the following sports (METs) and average activity speeds ($v_a$) (Ainsworth et al. 2000), with all clothing insulation set to 0.34 clo excluding football:

– Grass field: soccer (7 METs), $v_a = 3.0$ $ms^{-1}$
– Sand: beach volleyball (8 METs), $v_a = 1.0$ $ms^{-1}$
– Grass—park: walking (2.0 METs), $v_a = 2.0$ $ms^{-1}$
– School blacktop: basketball (8.0 METs), $v_a = 3.0$ $ms^{-1}$
– Artificial turf: American football (8.0 METs), $v_a = 0.3$ $ms^{-1}$ (Deren et al. 2014); clothing insulation = 0.62 clo (McCullough and Kenney 2003).
– Tennis court: tennis (5.0 METs), $v_a = 2.0$ $ms^{-1}$.

### Statistical evaluation and sensitivity testing

Although we attempt to complete a comparison of the different surfaces on the same tropical weather type days (largely DT), we experienced four MT weather types, including one overcast MT day. Therefore, to compare the different days and surface types in terms of their radiation balance, we calculated the $z$-scores of the ratio of $K_{in}$ to $L_{up}$ and $K_{in}$ to $Q^*$. This method allows for a standardized comparison between surfaces when higher $K_{in}$ values may have caused either high $L_{up}$ and/or high $Q^*$, as we only had one high-end weather station so it could not perform the direct simultaneous comparisons. Tests of linearity were performed on the relationships between $K_{in}$ versus $L_{up}$, and $K_{in}$ versus $Q^*$, displaying significant ($p < 0.05$) linearity and correlations ($r = 0.644$ and $0.805$, respectively).

Statistical evaluation of the three different methods to estimate the $R_{abs}$ was carried out by using mean bias error (MBE), mean absolute deviation (MAD), and root mean square error (RMSE), calculated as follows (Kenny et al. 2008):

$$MBE = \frac{\sum R_a - R_b}{n} \qquad (18)$$

$$MAD = \frac{\sum |R_a - R_b|}{n} \qquad (19)$$

$$RMSE = \sqrt{\frac{\sum (R_a - R_b)^2}{n}}, \qquad (20)$$

where $R_a$ and $R_b$ are the methods for estimating $R_{abs}$ and $n$ is the total number of measurements taken. All analyses and testing were completed in Python version 7.3-2 and SPSS version 24.

## Results

### Radiation and thermal microclimate

Table 2 presents a summary of the meteorological conditions present during each field deployment of the portable microclimate station. As the station was set up to represent a human, all values are at a height of 1.6 m for average human height. The greatest difference between the CRT temperature and $T_a$ ($\Delta T_{c-a} = T_{crt} - T_a$) was found over the sand (5.2 °C) and tennis court (3.3 °C), which indicates that there is a higher exchange of heat via free convection from the CRT. The remaining $\Delta T_{c-a}$ values ranged from 0.6–2.1 °C, thus indicating a lower convective heat exchange from the cylinder to the air. These observations indicate that the amount of convective heat transfer between the air and cylinder plays an important role in the calculation of $R_{crt}$, and is discussed further in "Sensitivity testing" section.

The four fluxes of radiation and the net radiation ($Q^*$) for each deployment are displayed in Fig. 2. The deployment on 7/14/14 was under overcast conditions with moist grass, and although the day was very hot (MT weather type), this surface presents a significantly lower radiation budget due to the clouds. Figure 2 displays the wide range of $K_{in}$ values between the non-overcast days (587.7–916.7 $Wm^{-2}$), which is primarily the result of varying minor intermittent cloud cover, and secondarily due to lower sun angles as the summer progressed (a slightly decreasing trend existed from the first (June 29) to the last deployment (Sept. 4), with 50-$Wm^{-2}$ difference from day 1 to day 13. As we ensured high SVFs, the variation in $Q^*$ was largely controlled by the $K_{in}$, with $L_{up}$ and $K_{up}$ also varying based on surface type, yet to a lesser extent. Due to the variability in $K_{in}$ by day, $z$-scores standardized by the $K_{in}$ are displayed for $Q^*$ and $L_{up}$. The

$z$-scores were not significantly above or below the mean, staying within ±2.0. The highest $Q^*$ values after standardizing for $K_{in}$ were over the sand, school blacktop, concrete, and both gray roof deployments. Without standardizing, we would have falsely concluded that the dry grass, artificial turf, and asphalt were the highest radiation budget (as indicated by the black bars), yet these high non-standardized $Q^*$ values are largely due to high $K_{in}$. The lowest $Q^*$ was found over wet grass and the three green roof deployments. The standardized $L_{up}$ values were highest over asphalt, sand, and green roof deployments 2 and 3, while low $L_{up}$ were found on gray roof 1, wet grass, the tennis court, and green roof 1.

Energy budgets calculated for a standing person over each surface were either "warm" or "hot" (+121 to +200 $Wm^{-2}$) (Brown and Gillespie 1986), with the vegetated roof surface resulting in the lowest energy budgets. These results align well with a similar study by Snir et al. (2016), who demonstrated a proportional relationship with vegetation and index of thermal stress in a given open location. When modeling an individual exercising, all estimates entered into the "hot" range (>250 $Wm^{-2}$) for exercising individuals (Kenny et al. 2009b). The $R_{abs}$ had the greatest influence on the energy budget estimates until a metabolic heat load was applied, at which point the metabolic heat load was the most important factor.

### Calculating radiation absorbed by a human

Values of $R_{abs}$ were calculated using the three methods outlined in the methodology using measurements from the net radiometer (CNR) and the CRT. Average values for all three methods are presented in Table 2 along with average $T_a$ (°C), CRT temperature (°C), $\Delta T_{c-a}$ (°C), and wind speed (ms$^{-1}$) over each surface.



**Fig. 2** Average values of incoming solar ($K_{in}$), reflected solar ($K_{up}$), incoming long-wave ($L_{in}$), outgoing long-wave ($L_{up}$), and net radiation ($Q^*$) in $Wm^{-2}$ on all surfaces. Standardized $L_{in}$ and $Q^*$ using $z$-scores are shown for comparative purposes
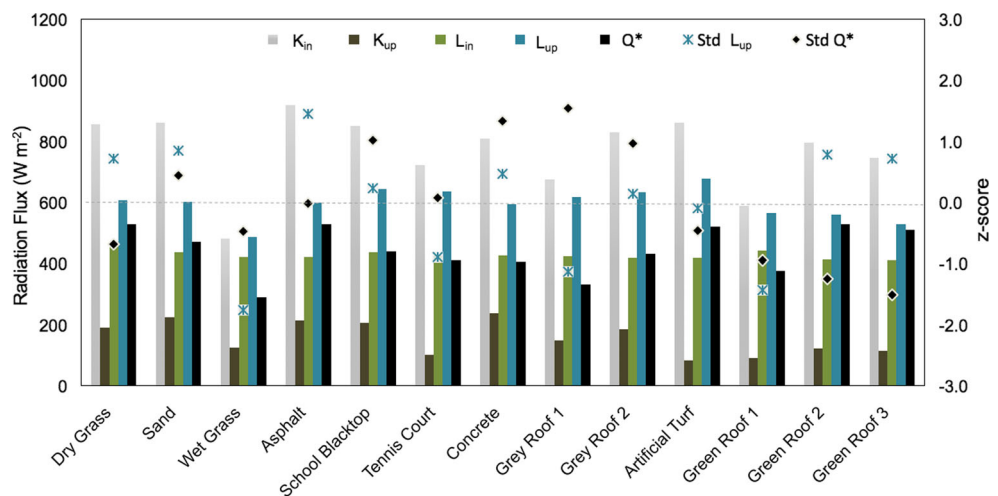
The $R_{cnr}$ method is considered the most accurate method to calculate $R_{abs}$ of those in this study because it uses direct measurements of the radiation components using advanced and high-cost research-grade instrumentation (Kenny et al. 2008). On average for all surfaces, estimates of $L_{abs}$ ($L_{up(abs)}$ plus $L_{in(abs)}$) from the CNR accounted for approximately 70% of the overall $R_{abs}$, with the remaining 30% from $K_{abs}$ (20% $K_{in(abs)}$ and 10% $K_{up(abs)}$). However, the influences of the surface on $R_{abs}$ is controlled by outgoing variables, with moderate variation found in the $L_{up(abs)}$ between surfaces, yet considerable variation in the $K_{up(abs)}$. This finding demonstrates the importance of albedo in altering the $R_{abs}$ by a human. The largest average $R_{cnr}$ values occurred over the dry grass, sand, school blacktop, concrete, and the gray roof, demonstrating $R_{cnr}$ values near or above 550 Wm$^{-2}$. The minimum average $R_{cnr}$ value was found over the wet grass due to constant cloud cover and lower surface temperatures of the moist grass.

Table 3 displays the statistical comparisons between the three methods used to calculate $R_{abs}$. When compared to the $R_{cnr}$ method, the CRT underestimated the $R_{abs}$ over all surfaces, excluding the sand surface (high $\Delta T_{c-a}$ and high $V$). The gray roof 1 deployment had the largest error between $R_{crt}$ and $R_{cnr}$, corresponding to the lowest $\Delta T_{c-a}$ (0.6 °C). The deployments with an error value above 15% had minor intermittent cloud cover throughout the deployment. As demonstrated in Fig. 3, the $R_{crt}$ responded moderately well to the minor intermittent cloud cover during the overall clear day, yet the response is also lagged as compared to the CNR, as was highly affected by wind; both $T_{crt}$ and wind speed sensitivity factors are assessed alone in "Sensitivity testing" section.

Figure 3 displays the $R_{abs}$ values for the sand and tennis court surfaces. The $R_{abs}$ values range from 400 and 750 Wm$^{-2}$ and peaks between 14:35 and 14:50 and at 16:50 for sand. The tennis court does not have a discernible peak in $R_{cnr}$ because of the minor intermittent cloud cover that causes large variations in the $R_{abs}$ values. Clouds have some effect on $R_{crt}$ as can be seen in the decreases in $R_{crt}$ that coincide with decreases in $R_{cnr}$. One example of this occurs at approximately 15:11 over the tennis court (Fig. 3a). When a cloud passes over, the CRT temperature decreases which lessens the amount of convective heat transfer between the cylinder and the air. $R_{crt}$ presents the most variability of all methods even under clear skies due to it depending on the measurements of $T_a$, $T_{crt}$, and most importantly the wind speed. All deployments showed a trend of $R_{cnr}$ and $R_{est}$ decreasing as the sun lowers on the horizon and as a result the cylinder receives less incoming solar radiation. $K_{in(abs)}$ is the only component of $R_{cnr}$ that decreases in the late afternoon and is responsible for this gradual dip in $R_{cnr}$ values.

## Sensitivity testing

To assess the errors between the three methods, a sensitivity analysis was performed on Eq. 15. $R_{crt}$ is calculated based on a complex interaction of sensible heat transfer, the resistance of the cylinder to that heat transfer, and the amount of long-wave radiation emitted by the cylinder. This analysis shows how changes in the meteorological inputs (i.e., $T_a$, $T_{crt}$, and wind speed) affect the calculation of $R_{abs}$ using the CRT and further identify suitable meteorological conditions for using the CRT. Base values for the sensitivity analysis

**Table 3** Statistical evaluation of the differences in the three $R_{abs}$ methods. RMSE (%) is the percent of the mean of two variables analyzed

| Surface | MBE (Wm$^{-2}$) | MAD (Wm$^{-2}$) | RMSE (Wm$^{-2}$) | RMSE (%) | % error |
|---|---|---|---|---|---|
| $R_{crt} - R_{cnr}$ | | | | | |
| Dry grass | −92.7 | 93.3 | 96.6 | 19.3 | 20.3 |
| Sand | 90.3 | 90.3 | 99.7 | 16.6 | −13.9 |
| Wet grass | −40.9 | 41.7 | 59.1 | 13.9 | 10.0 |
| Asphalt | −85.7 | 85.7 | 88.2 | 17.7 | 18.8 |
| School blacktop | −88.2 | 90.0 | 94.4 | 18.4 | 18.7 |
| Tennis court | −33.5 | 46.6 | 54.2 | 10.5 | 6.6 |
| Concrete | −91.7 | 91.7 | 94.9 | 18.8 | 20.1 |
| Gray roof 1 | −102.3 | 102.5 | 110.1 | 23.2 | 24.1 |
| Gray roof 2 | −153.0 | 153.0 | 154.1 | 32.0 | 37.7 |
| Artificial turf | −70.5 | 70.5 | 72.0 | 14.0 | 11.5 |
| Green roof 1 | −47.8 | 58.5 | 76.3 | 15.9 | 10.4 |
| Green roof 2 | −63.3 | 63.3 | 65.9 | 13.4 | 13.7 |
| Green roof 3 | −95.8 | 97.1 | 106.0 | 21.8 | 21.7 |
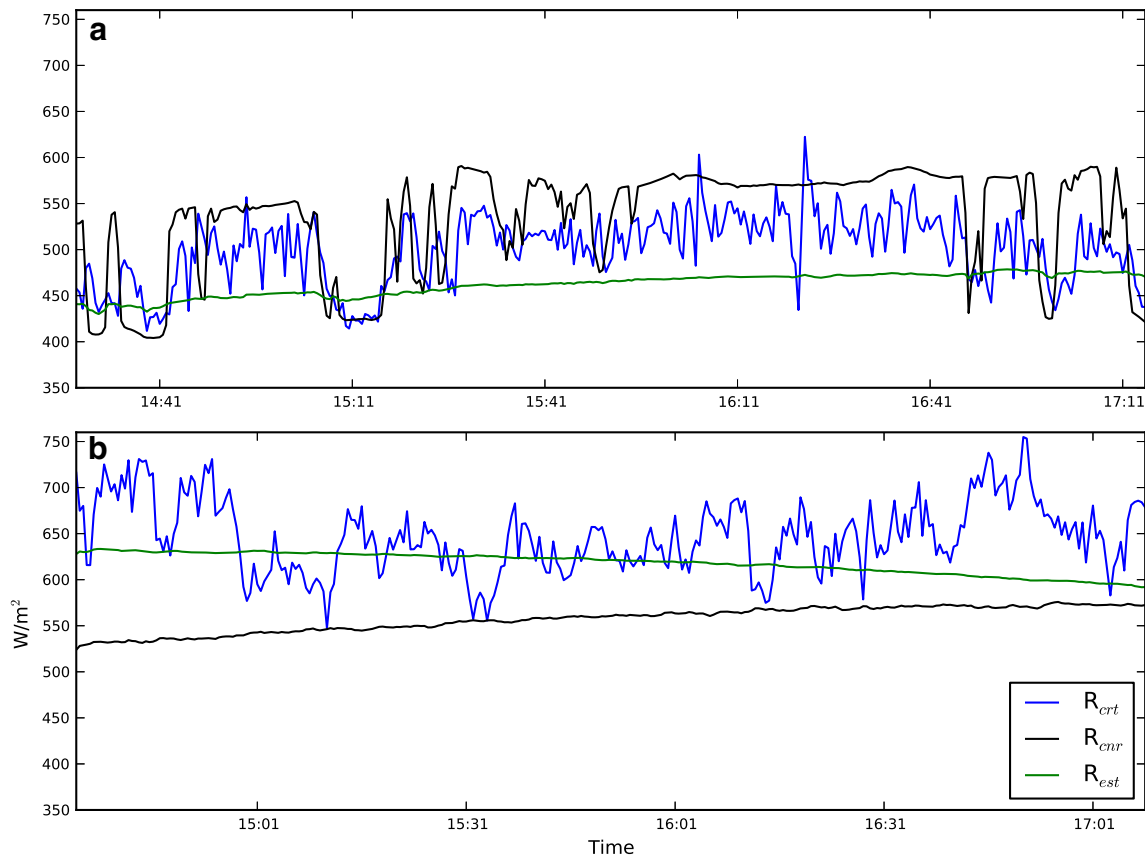
**Fig. 3** Time series of $R_{cnr}$ (*black*), $R_{crt}$ (*blue*), and $R_{est}$ (*green*) over tennis court (**a**) and sand (**b**)

were obtained by calculating the averages of all surfaces for $T_{crt}$, $T_a$, $\Delta T_{c-a}$, $r_m$, and $V$. Each of the input variables were changed using the following ranges and increments:

- $T_a = 27$–$47$ °C at increments of 0.1 °C
- $T_{crt} = 27$–$47$ °C at increments of 0.1 °C
- $\Delta T_{c-a} = -1.0$–$10$ °C at increments of 0.1 °C
- $r_m = 10.0$–$146$ sm$^{-1}$ at increments of 1 sm$^{-1}$
- $V = 0.0$–$10.0$ ms$^{-1}$ at increments of 0.05 ms$^{-1}$.

Figure 4 displays the results of all sensitivity tests for the listed variables. Responses of $T_{crt}$, $T_a$, and $\Delta T_{c-a}$ display linearity with $R_{crt}$, with $T_a$ showing an inverse relationship (Fig. 4a, b, c). With all other variables held constant, an increase in $T_a$ of 1.0 °C resulted in a 23.8 Wm$^{-2}$ decrease in $R_{crt}$ due to a lower $\Delta T_{c-a}$, and thus a lower convective term in Eq. 15, which is also shown by the similar but positive linear relationship of $R_{crt}$ to $\Delta T_{c-a}$ in plot C. The $R_{crt}$ was particularly sensitive to $T_{crt}$, where an increase of 1 °C resulted in an increase of $R_{abs}$ by 28.8 Wm$^{-2}$. The $T_{crt}$ is weighted more heavily in Eq. 15 as it is used in both terms (emitted long-wave radiation and sensible heat transfer).

The sensitivity between wind speed and $r_m$ (Fig. 4d, e) has a largely non-linear relationship with $R_{crt}$, although above 2 ms$^{-1}$, the relationship is nearly linear (Fig. 4d).

$R_{crt}$ is the most sensitive to wind speed between 0–1 ms$^{-1}$ within which $R_{crt}$ changes by 50 Wm$^{-2}$; however, between 1 and 10 ms$^{-1}$, the $R_{crt}$ has a step change of 14 Wm$^{-2}$ per 1 ms$^{-1}$. The sensitivity analysis of $R_{crt}$ to $r_m$ shows a strong exponential decrease in $R_{crt}$ with increasing resistance values (Fig. 4e). $R_{crt}$ is the most sensitive between $r_m$ values of 0–40 sm$^{-1}$ where there is net change in absorbed radiation of 130 Wm$^{-2}$ compared to a change of 30 Wm$^{-2}$ between 40 and 146 sm$^{-1}$. The sensitivity of $r_m$ to wind speed is shown in Fig. 4f, where there is a large exponential decrease in $r_m$ between 0 and 1 ms$^{-1}$. This decrease has a large influences on the $R_{abs}$, causing a step change of 110 Wm$^{-2}$, whereas at wind speeds between 1 and 10 ms$^{-1}$, the $R_{abs}$ varies by only 24 Wm$^{-2}$ throughout the full range.

While both wind speed and $\Delta T_{c-a}$ modulate $R_{crt}$, the $\Delta T_{c-a}$ plays the larger role out of the two, and a low $\Delta T_{c-a}$ may be the cause of a higher error. For example, a decrease in $\Delta T_{c-a}$ explains 61% of the percent error results in Table 3 using linear regression, while the relationship between wind speed and percent error provided a coefficient of determination of 0.01. However, numerous other parameters affect the variables within Eq. 13, yet a higher $\Delta T_{c-a}$ directly results in less error from the $R_{cnr}$ estimates.
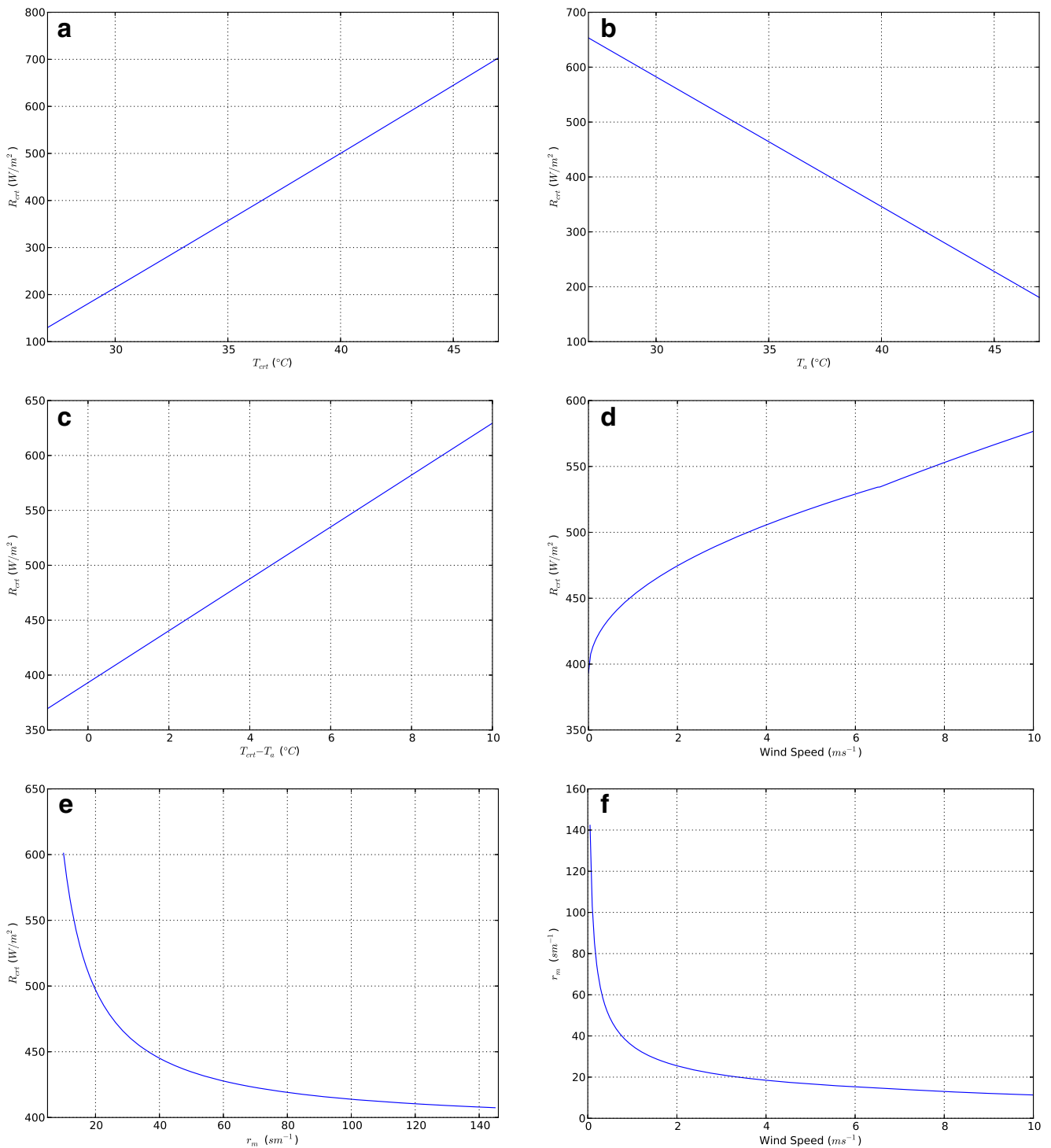
**Fig. 4** Sensitivity of $R_{crt}$ to CRT temperature (**a**), air temperature (**b**), difference between $T_{crt}$ and $T_a$ (**c**), wind speed (**d**), and resistance of a cylinder to heat transfer (**e**). Sensitivity of resistance of cylinder to wind speed (**f**)

## Discussion

The current study examined the radiation environment and thermal energy budget experienced by a model human over ten common urban surfaces during extreme heat conditions

($T_a > 38$ °C) on predominantly clear days in Lubbock, Texas, using three methods: estimation, net radiometer, and cylindrical radiation thermometer. The net radiometer provides the most accurate measurements of the four components of radiation, and hence, the most accurate $R_{abs}$ value.

## Radiative fluxes and urban heat mitigation potential

An integrated estimation of the short- and long-wave radiation fluxes into one value (such as $T_{mrt}$ or $R_{abs}$) is an important parameter to use and understand when implementing UHI mitigation measures in urban and landscape planning (Matzarakis et al. 2007). Such measures often focus on reducing heat gain to the urban fabric and lowering surface temperature and sensible heat flux. The current study showed that the surface type altered the values of $K_{up}$ and $L_{up}$, with a larger influence on $K_{up}$; however, the decreased surface temperature from a higher albedo may be offset by increased solar radiation reflected by the surface, as also found by Erell et al. (2014). These relatively low-albedo surfaces resulted in relatively lower $K_{up}$ values (e.g., artificial turf with a 0.09 albedo and $K_{up}$ of 89 Wm$^{-2}$). However, a higher albedo increases the amount of reflected solar, and thus the $K_{up}$ absorbed by a human. For example, we found that for surfaces with albedos >0.22 and on the clearest days ($\tau$ >60%), the average $K_{up}$ imposed on a human was 209 Wm$^{-2}$, as compared to 105 Wm$^{-2}$ on lower-albedo surfaces and clear days. However, there was minimal difference in the standardized $L_{up(abs)}$, signifying that a change in albedo has the greatest acute effect on $K_{up}$, which acts to increase the overall $R_{abs}$ by a human. This increase directly causes a decline in thermal comfort, as found by Middel et al. (2016) in sunny, hot conditions.

The thermal influences of $K_{up}$ align well with that found by Erell et al. (2014), which suggested that the reduction in albedo in canyons is not enough to offset increased radiant loads on a human in an urban environment. A recent study by Taleghani et al. (2016) also found that incorporating solar reflective cool pavements may increase the $T_{mrt}$ based on a modeled environment, thus decreasing comfort (based on the PET model; Matzarakis et al. (2007)). Although reducing the heat absorbed into city fabric through lower albedos is an important UHI mitigation technique—particularly for overnight temperatures—it may not considerably improve human thermal comfort since the $K_{up}$ imposed on a human increases and the $L_{up}$ is less sensitive. It must be noted that our observations are only for high SVF conditions which are less common in cities (other than rooftops), but allow us to better understand independently how the surface type affects human thermal comfort, which differs from understanding the influence of radiation on energy usage in buildings. The current study also has strength in assessments under real-world conditions that allow the quantification of cumulative effects on the surface in direct afternoon sun (e.g., thermal inertia).

A study by Lindberg et al. (2016) also assessed the influence of ground surface on $T_{mrt}$ using the SOLWEIG model and simultaneous observations over grass and asphalt, finding the $T_{mrt}$ during heat-wave episodes to be higher over the asphalt in full sunlit locations. However, there was a minimal difference in the albedos (0.16 versus 0.18 for asphalt and grass, respectively), and thus, the reduced $T_a$ over the moist grass aids in reducing the heat load. Results from the current study, as well as those by Taleghani et al. (2016) and Lindberg et al. (2016), and Erell et al. (2014), demonstrate that low-albedo strategies on dry surfaces may not improve the thermal comfort as expected, and that energy partitioning into latent heat (using vegetation or water) may be a more important focus in improving thermal comfort in the daytime.

Past work by Bowler et al. (2010), Golden (2004), and Rosenzweig and Solecki (2006) show that green roofs and green areas can reduce air temperature in cities. Hot and arid locations can benefit the greatest from techniques that reduce the radiation absorbed by the urban fabric—thus reducing the $R_{abs}$ by a human—where employing shade and/or transpirational cooling can significantly lower surface temperatures and sensible heating, thus the $K_{up}$ and $L_{up}$ from a surface. Effective urban greenspace (with shade and moisture) can improve the frequency and amount of active use in urban parks (Lin 2009; Thorsson et al. 2007; Thorsson et al. 2004), environmental valuation and aesthetics of a neighborhood (Knez and Thorsson 2006), as well as thermal comfort and heat stress (Ketterer and Matzarakis 2014; Vanos 2015). An example of this in the current study is demonstarted by the vegetated surfaces being much cooler than artificial turf, which was found to have the most extreme conditions at the surface (highest $L_{up}$ of 675 Wm$^{-2}$, and a surface temperature of 78 °C), slightly higher than that found by Snir et al. (2016). The blacktop, gray roof, and tennis court also displayed $L_{up}$ values above 630 Wm$^{-2}$.

While thermal discomfort was predominant when modeling a human's heat balance based on a standing MET, heat stress was found to be a large concern based on the modeling of individuals using sport-specific metabolic activity levels and clothing inputs. In all energy budget estimations during physical activity (excluding the cloudy day), the athletes would have been entering a range of incompensable exertional heat stress. As the given days were near heat-warning thresholds and monitoring took place midday, it is unlikely that many individuals would attempt to perform such activities. Nonetheless, the example provided here displays a method of estimating heat stress during high METs on hot days, why high MET activity should be avoided or limited, and of modeling the influence of possible design changes on thermal comfort. Such an example is also provided by Grundstein et al. (2017) for exertional heat illness in americna football.

Finally, results from the current study show that green roofs, even if not fully vegetated, effectively mitigate the radiation budget of a surface ($Q^*$). Green roofs are a

promising cooling technique for UHI heat island mitigation and lowered energy use (Santamouris 2014). The cooling provided can be enhanced through shade; hence, a future empirical study comparing surface type impacts on the various human energy budget fluxes under both sun-exposed and shaded conditions and in canyon and open conditions is important future research.

### Estimating the radiation absorbed by a human

In comparing the three methods of estimating radiation absorbed by a human, we found that the $R_{crt}$ is largely sensitive to $\Delta T_{c-a}$ and wind speed. Percent errors between the various methods are generally acceptable within 10% of $R_{cnr}$ (Krys and Brown 1990) as challenges exist with respect to the accurate data collection of short- and long-wave radiation measurements, with lags often present in instruments, and with the inherent difficulty in measuring all meteorological variables. The value of 10% from Krys and Brown (1990) also corresponds to a narrow range of fair weather clear conditions in short timespans, and thus, the current testing provides information on the CRT performance in a wider range of conditions with some minor intermittent cloud cover during the overall clear days. Intermittent cloud cover may introduce errors between the two methods as the cylinder has a steady state output, so there may be a delayed response of the CRT temperature to cloud cover (Kenny et al. 2008). Averaging data over 5 min prior to RMSE and percent error calculations as in Kenny et al. (2008) would greatly diminish said errors. The CNR detects and models this change at a very high temporal resolution (1 s), yet the CRT can take up to 6min to adapt to this change, and therefore, disagreement may be present on days of intermittent clouds due to this lag in the CRT. This notion of errors due to slower response time is supported further by results showing that the $\Delta T_{c-a}$ may be a more important factor than the wind. Research is ongoing to determine the response time of the CRT, and thus, determine accurate lag corrections or averaging windows. As compared to other low-cost radiation instruments (such as the 20-min response time of the black globe thermometer; Kántor and Unger (2011)), a 4–6-min lagged time is a significant improvement for low-cost radiational monitoring. Further, measurements under nondynamic conditions or in environments primarily composed of diffuse radiation, as presented by Krys and Brown (1990), we would also expect to find closer agreement between $R_{crt}$ and $R_{cnr}$. The low errors under cloudy conditions support this finding.

Although maintaining a relatively stationary environment with no change in surface type or shade (other than intermittent clouds at times) allowed for the comparisons by surface type, direct comparisons could be accomplished with multiple high-end weather stations over the various surfaces simultaneously; however, this would be costly. Validating low-cost solutions to monitoring the radiational environment (such as the CRT or the gray globe thermometer; Thorsson et al. (2007) and Johansson et al. (2014)) is an important future research direction to support accurate $T_{mrt}$ and $R_{abs}$ measurements throughout urban areas. Since the notion of using a cylinder for $T_{mrt}$ calculations for a human was introduced, it is continually applied in observational and modeling studies by others (e.g., Erell et al. 2014; Kántor et al. 2014; Thorsson et al. 2007; Holmer et al. 2015). Further studies assessing the usefulness of such instruments in shaded and sun exposures would provide critical information on the value of shade in addition to surface selection for thermal comfort and UHI mitigation.

## Conclusions

Human exposure to hot weather is an increasingly important public health concern, particularly in cities dominated by impervious materials absorbing and re-emitting high loads of radiant energy. The purpose of the current study was to assess the changes in the absorbed radiation by a human—an important component of human energy budget models—over varying urban surface types with high SVFs on hot summer days. Field tests conducted using a high-end microclimate station suggest that although high-albedo surfaces may help reduce the UHI intensity, they may not improve acute human thermal comfort due to increased reflected outgoing radiation that affects the amount of radiation a human body absorbs. Atmospheric transmissivity controls the incoming radiation and thus a large proportion of the overall $R_{abs}$, yet the variability of reflected radiation plays a key role in $R_{abs}$. A future study simultaneously assessing combinations of surface and shade types in clear conditions can better assess radiant differences under similar atmospheric conditions to evaluate the effects on $R_{abs}$.

To examine the potential for low-cost and less-complex measurement opportunities of $R_{abs}$ or $T_{mrt}$ measurements, two methods (a CRT instrument and theoretical modeling) were compared to the $R_{abs}$ values produced using a single high-end net radiometer. Sensitivity testing of data collected at a high sampling frequency revealed that absorbed radiation by the CRT is highly sensitive to wind speed and the differential between $T_a$ and $T_{crt}$, with the largest errors attributable to wind speeds <2 ms$^{-1}$ and low amounts of sensible heat transfer based on $\Delta T_{c-a}$ differences. It is recommended that for further use of the CRT, data should use collection intervals or smoothed averages at 5 min or greater (as opposed to 30 s used here).

Given that an important reason for mitigating the UHI is to lessen heat stress on humans, and that radiation is

often the main contributor of heat gain to humans in hot, clear conditions, then it follows that urban design decisions can benefit from fine-scale observations of $R_{abs}$. However, the choice for dry heat mitigation techniques (i.e., not considering vegetation or water) is highly dependent on the combined consideration of the purpose of the space (i.e., human use or not) and timescale of its use, such as improving the short-term thermal comfort, or reducing cumulative heat gain to buildings. Gaining a fuller understanding of the various and distinct microclimates present throughout a city (i.e., rooftops and canyons), their intended use, and their radiant and thermal properties can help improve the benefits of targeted urban climate adaptation.

# References

Ainsworth BE, Haskell WL, Whitt MC, Irwin ML, Swartz AM, Strath SJ, O'Brien WL (2000) Compendium of physical activities: an upyear of activity codes and MET intensities. Med Sci Sport Exer 32(9):498–516

Berko J, Ingram D, Saha A, Parker J (2014) Deaths attributed to heat, cold, and other weather events in the United States, 2006–2010. Tech. Rep. 76, National Center for Health Statistics

Bowler DE, Buyung-Ali L, Knight TM, Pullin AS (2010) Urban greening to cool towns and cities: a systematic review of the empirical evidence. Landsc Urban Plan 97(3):147–155

Brock F, Richardson S (2001) Meteorological measurement systems. Oxford University Press

Brown RD, Gillespie TJ (1986) Estimating outdoor thermal comfort using a cylindrical radiation thermometer and an energy budget model. Int J Biometeorol 30(1):43–52

Brown RD, Gillespie TJ (1995) Microclimate landscape design. John Wiley & Sons, Inc

Campbell G (1977) An introduction to environmental biophysics. Springer, New York

Campbell G, Norman J (1998) An introduction to environmental biophysics. Springer, New York Berlin Heidelberg

Chen L, Ng E, An X, Ren C, Lee M, Wang U, He Z (2012) Sky view factor analysis of street canyons and its implications for daytime intra-urban air temperature differentials in high-rise, high-density urban areas of Hong Kong: a GIS-based simulation approach. Int J Climatol 32(1):121–136

Chow WTL, Brennan D, Brazel AJ (2012) Urban heat island research in Phoenix, Arizona: theoretical contributions and policy applications. Bull Am Meteorol Soc 93(4):517–530

Deren TM, Coris EE, Casa DJ, DeMartini JK, Bain AR, Walz SM, Jay O (2014) Maximum heat loss potential is lower in football linemen during an NCAA summer training camp because of lower self-generated air flow. J Strength Cond Res 28(6):1656–1663

Erell E, Pearlmutter D, Boneh D, Kutiel PB (2014) Effect of high-albedo materials on pedestrian heat stress in urban street canyons. Urban Climate 10:367–386

Fanger PO (1970) Thermal comfort. Analysis and application in environmental engineering. Danish Technical Press, Copenhagen

Golden JS (2004) The built environment induced urban heat island effect in rapidly urbanizing arid regions—a sustainable urban engineering complexity. Environ Sci 1(2013):321–349

Grimm NB, Faeth SH, Golubiewski NE, Redman CL, Wu J, Bai X, Briggs JM (2008) Global change and the ecology of cities. Science 319(5864):756–760

Grimmond CSB, Roth M, Oke TR, Au YC, Best M, Betts R, Carmichael G, Cleugh H, Dabberdt W, Emmanuel R, Freitas E, Fortuniak K, Hanna S, Klein P, Kalkstein LS, Liu CH, Nickson A, Pearlmutter D, Sailor D, Voogt J (2010) Climate and more sustainable cities: climate information for improved planning and management of cities (Producers/Capabilities Perspective). Procedia Environ Sci 1:247–274

Grundstein A, Knox JA, Vanos J, Cooper ER, Casa DJ (2017) American football and fatal exertional heat stroke: a case study of Korey Stringer. Int J Biometeorol 1–10

Harlan SL, Brazel AJ, Prashad L, Stefanov WL, Larsen L (2006) Neighborhood microclimates and vulnerability to heat stress. Soc Sci Med 63:2847–2863

Holmer B, Lindberg F, Rayner D, Thorsson S (2015) How to transform the standing man from a box to a cylinder—a modified methodology to calculate mean radiant temperature in field studies and models. In: ICUC9 - 9th international conference on urban climate. Toulouse, France

ISO9920 (2007) ISO 9920: Ergonomics of the thermal environment: estimation of the thermal insulation and water vapour resistance of a clothing ensemble. ISO, Geneva

Jenerette G, Harlan S, Buyantuev A, Stefanov W, Declet-Barreto J, Ruddell B, Myint S, Kaplan S, Li X (2015) Micro scale urban surface temperatures are related to land cover features and residential heat-related health impacts in Phoenix, AZ USA. Landscape Ecology. https://doi.org/10.1007/s10980-015-0284-3

Johansson E, Thorsson S, Emmanuel R, Krüger E (2014) Instruments and methods in outdoor thermal comfort studies—the need for standardization. Urban Climate 10:346–366

Kántor N, Lin TP, Matzarakis A (2014) Daytime relapse of the mean radiant temperature based on the six-directional method under unobstructed solar radiation. Int J Biometeorol 58:1615–1625

Kántor N, Unger J (2011) The most problematic variable in the course of human-biometeorological comfort assessment—the mean radiant temperature. Central European Journal of Geosciences 3(1):90–100

Kenny NA, Warland JS, Brown RD, Gillespie TG (2008) Estimating the radiation absorbed by a human. Int J Biometeorol 52(6):491–503

Kenny NA, Warland JS, Brown RD, Gillespie TG (2009a) Part A: Assessing the performance of the COMFA outdoor thermal comfort model on subjects performing physical activity. Int J Biometeorol 53:415–428

Kenny NA, Warland JS, Brown RD, Gillespie TG (2009b) Part B: revisions to the COMFA outdoor thermal comfort model for application to subjects performing physical activity. Int J Biometeorol 53:429–441

Ketterer C, Matzarakis A (2014) Human-biometeorological assessment of heat stress reduction by replanning measures in Stuttgart, Germany. Landsc Urban Plan 122:78–88

Knez I, Thorsson S (2006) Influences of culture and environmental attitude on thermal, emotional and perceptual evaluations of a public square. Int J Biometeorol 50(5):258–268

Kreith F, Black W (1980) Basic heat transfer. Harper and Row, New York

Krüger E, Drach P, Emmanuel R, Corbella O (2013) Urban heat island and differences in outdoor comfort levels in Glasgow, UK. Theor Appl Climatol 112(1-2):127–141

Krys Sa, Brown RD (1990) Radiation absorbed by a vertical cylinder in complex outdoor environments under clear sky conditions. Int J Biometeorol 34(2):69–75

Kuras E, Bernhard M, Calkins M, Ebi K, Hess J, Kintziger K, Jagger M, Middel A, Scott A, Spector J, Uejio C, Vanos J, Zaitchik B, Gohlke J, Hondula D (2017) Opportunities and challenges for personal heat exposure research. Environmental Health Perspectives

Kuras ER, Hondula DM, Brown-Saracino J (2015) Heterogeneity in individually experienced temperatures (IETs) within an urban neighborhood: insights from a new approach to measuring heat exposure. Int J Biometeorol 1–10

Lin T (2009) Thermal perception, adaptation and attendance in a public square in hot and humid regions. Build Environ 44(10):2017–2026

Lindberg F, Onomura S, Grimmond C (2016) Influence of ground surface characteristics on the mean radiant temperature in urban areas. Int J Biometeorol 1–14

Matzarakis A, Muthers S, Koch E (2011) Human biometeorological evaluation of heat-related mortality in Vienna. Theor Appl Clim 105:1–10

Matzarakis A, Rutz F, Mayer H (2007) Modelling radiation fluxes in simple and complex environments, application of the RayMan model. Int J Biometeorol 51(4):323–334

McCullough EA, Kenney WL (2003) Thermal insulation and evaporative resistance of football uniforms. Med Sci Sports Exerc 35(5):832–837

Middel A, Häb K, Brazel AJ, Martin CA, Guhathakurta S (2014) Impact of urban form and design on mid-afternoon microclimate in phoenix local climate zones. Landsc Urban Plan 122:16–28

Middel A, Selover N, Hagen B, Chhetri N (2016) Impact of shade on outdoor thermal comfort—a seasonal field study in Tempe, Arizona. Int J Biochem 1–13

Monteith J (1973). In: Edward Arnold (ed) Principles of environmental physics, 1st edn. MA, Burlington

Monteith J, Unsworth M (1990) Principles of environmental physics, 2nd edn. Butterworth-Heinemann, Boston, MA

Monteith J, Unsworth M (2008) Principles of environmental physics, 3rd edn. Elsevier, Burlington, MA

Oke T (1987) Boundary layer climates, 2nd edn. Routledge, New York

Oke T, Zeuner G, Jauregui E (1992) The surface energy balance in Mexico City. Atmos Environ Part B 26(4):433–444

Rosenzweig C, Solecki W (2006) Mitigating New York City's heat island with urban forestry. Living Roofs and Light Surfaces, New York, pp 1–5

Santamouris M (2014) Cooling the cities—a review of reflective and green roof mitigation technologies to fight heat island and improve comfort in urban environments. Sol Energy 103:682–703. https://doi.org/10.1016/j.solener.2012.07.003. http://www.sciencedirect.com/science/article/pii/S0038092X12002447

Sheridan SC (2002) The redevelopment of a weather-type classification scheme for North America. Int J Climatol 22(1):51–68

Snir K, Pearlmutter D, Erell E (2016) The moderating effect of water-efficient ground cover vegetation on pedestrian thermal stress. Landsc Urban Plan 152:1–12

Solís P, Vanos JK, Forbis RE (2016) The decision-making/accountability spatial incongruence problem for research linking environmental science and policy. Geographical Review

Steeneveld G, Koopmans S, Heusinkveld B, Van Hove L, Holtslag A (2011) Quantifying urban heat island effects and human comfort for cities of variable size and urban morphology in the Netherlands. J Geophys Res Atmos 116(D20)

Taleghani M, Sailor D, Ban-Weiss GA (2016) Micrometeorological simulations to predict the impacts of heat mitigation strategies on pedestrian thermal comfort in a los angeles neighborhood. Environ Res Lett 11(2)

Tan J, Zheng Y, Tang X, Guo C, Li L, Song G, Zhen X, Yuan D, Kalkstein AJ, Li F (2010) The urban heat island and its impact on heat waves and human health in Shanghai. Int J Biometeorol 54(1):75–84

Theeuwes NE, Steeneveld GJ, Ronda RJ, Rotach MW, Holtslag AA (2015) Cool city mornings by urban heat. Environ Res Lett 10(11):114,022

Thorsson S, Lindberg F, Eliasson I, Holmer B (2007) Different methods for estimating the mean radiant temperature in an outdoor urban setting. Int J Climatol 27(14):1983–1993

Thorsson S, Lindqvist M, Lindqvist S (2004) Thermal bioclimatic conditions and patterns of behaviour in an urban park in Goteborg, Sweden. Int J Biometeorol 48:149–156

van den Brink A, Bruns D, Tobi H, Bell S (2016) Research in landscape architecture: methods and methodology. Taylor & Francis. https://books.google.com/books?id=cTR6DQAAQBAJ

Vanos J, Warland J, Gillespie T, Kenny N (2012a) Thermal comfort modelling of body temperature and psychological variations of a human exercising in an outdoor environment. Int J Biometeorol 56(1):21–32

Vanos J, Warland J, Gillespie T, Kenny N (2012) Thermal comfort modelling of body temperature and psychological variations of a human exercising in an outdoor environment. Int J Biometeorol 56(1):21–32

Vanos JK (2015) Childrens health and vulnerability in outdoor microclimates: a comprehensive review. Environ Int 76:1–15

Vanos JK, Middel A, McKercher G, Kuras ER, Ruddell B (2016) Hot playgrounds and childrens health: a multiscale analysis of surface temperatures in Arizona, USA. Landsc Urban Plan 146:29–42. https://doi.org/10.1016/j.landurbplan.2015.10.007

Vanos JK, Warland JS, Gillespie TJ, Kenny NA (2012) Improved predictive ability of climate-human-behaviour interactions with modifications to the COMFA outdoor energy budget model. Int J Biometeorol 56(6):1065–74

Vanos JK, Warland JS, Kenny NA (2010) Review of the physiology of human thermal comfort while exercising in urban landscapes and implications for bioclimatic design. Int J Biometeorol 54(4):319–334